3-ISL Topology: Routing Properties and Performance in LEO Mega-Constellation Networks

Quan Chen, Lei Yang, Yong Zhao, Yi Wang, Haibo Zhou, and Xiaoqian Chen

***Abstract*—Mega-constellation networks widely employ inter-satellite links (ISLs) to enhance network connectivity. However, the ISLs, particularly the inter-plane ISLs that span different orbital planes, are dynamic and difficult to maintain. The inter-plane ISLs are less used and can be partly saved. Recently, a special ISL configuration with pruned inter-plane ISLs has been implemented in Starlink, yet less studied. This paper delves into the topological characteristics and routing issues of this pruned ISL pattern, specifically the 3-ISL topology. This topology is mathematically modeled and indexed, and key routing properties are derived, including the minimum hop-count, network diameter, network cost, and average path length of the 3-ISL topology. These fundamental properties are rigorously proven for both Mesh and Torus topologies. Additionally, the shortest path searching region and path diversity are deduced. Numerical simulations verify these propositions, and the results of mega-constellation scenarios suggest that pruning ISLs could lead to increased path distance, higher delay, and reduced network capacity. However, in certain constellation configurations, some metrics are comparable to those of the traditional 4-ISL topology, thereby potentially reducing system costs. Constellations with fewer orbital planes and more satellites in each plane are less affected by pruning ISLs and thus preferred. The findings can provide analytic insights for routing strategies and guide the integrated design of constellation configuration and ISL topology.**

***Index Terms*—Routing property, 3-ISL topology, LEO constellation networks, Starlink, Pruned inter-satellite link**

I. Introduction

Low Earth orbit (LEO) mega-constellation networks, represented by Starlink, OneWeb, and Kuiper, have become an emerging hot area in communication networks and the Internet [1]. To enhance the network connection, satellites in mega-constellations are equipped with inter-satellite links (ISLs), forming a global internet mesh for user access [2], [3]. Transmission through ISLs also causes inter-satellite routing issues, where the algorithm and performance are closely related to topological configuration [4].

This work was supported in part by the National Natural Science Foundation of China (Grant No. 62401597), the Natural Science Foundation of Hunan Province, China (Grant No. 2024JJ6469), and in part by Scientific Research Project of National University of Defense Technology (No. ZK22-02). (Corresponding author: Quan Chen)

Q. Chen, L. Yang, and Y. Zhao are with the College of Aerospace Science and Engineering, National University of Defense Technology, Changsha 410073, China. (Email: {chenquan11@foxmail.com; craftyang@163.com; zhaoyong@nudt.edu.cn})

Y. Wang is with the Nanjing Research Institute of Electronics Technology, Nanjing 210013, China. (Email: wangyi15@nudt.edu.cn)

H. Zhou is with the School of Electronic Science and Engineering, Nanjing University, Nanjing 210023, China. (Email: haibozhou@nju.edu.cn)

X. Chen is with the Chinese Academy of Military Science. (Email: chenxiaoqian@nudt.edu.cn)

In most academic studies and actual constellation design proposals with ISLs, each satellite is designed with four ISLs connecting its neighbors in front, rear, left, and right, i.e., two intra-plane ISLs and two inter-plane ISLs [5]–[9]. The 4-ISL pattern topology is also named the '+Grid' or 'X' pattern, represented by the Iridium system [5]. The 4-ISL configuration transforms the network into a regular Mesh or Torus topology [10].

For 4-ISL topology, its topological features, routing properties, and capacity issues have been proven and well investigated [11]–[14]. Facilitated by satellite indexing, the minimum hop-count can be calculated and many routing schemes are proposed [15], [16]. The shortest routing can be confined to a grid-like subgraph, and the potential next hop directions towards the destination are unambiguous. Lu et al. [14] derive the average path length in the 4-ISL network which increases with the constellation scale, and propose a structural optimization method to enhance the transmission efficiency of mega-constellation. The seam in polar constellations may transform the 4-ISL tours into Semi-Mesh, then Wang et al. [17] propose an encountering ISL pattern and derive minimum hop-count formula. The node failure issue and topology robustness are also studied [18]–[20]. Lai et al. [21] further propose a resilient routing to eliminate the topological uncertainty caused by LEO dynamics and uncertain failures.

By exploiting the symmetric and regular 4-ISL topology of LEO mega-constellation, Chen et al. [22] have proved the explicit relations between the minimum hop path and shortest distance path and propose an analytic end-to-end hop-count evaluation method with high accuracy [9]. Furthermore, by combining the inter-plane ISL features, they also propose an explicit shortest path algorithm [12], which indicates that the exploitation of the topological features can facilitate routing scheme design, improve routing efficiency, and reveal networking characteristics.

However, due to the relative high-speed satellite movement, the inter-plane ISLs between two orbit planes are much more dynamic than intra-plane ISLs [23]. The maintenance of inter-plane ISL is much more challenging and costly, and the transmission through inter-plane would be unreliable and cause instability to the end-to-end routing. Thus, minimizing the usage of inter-plane ISL is desired [23], [24]. And the inter-plane ISL terminals can be partly saved to reduce the cost.

Therefore, the ISL topology with pruned inter-plane ISLs becomes a promising solution and have been implemented in practice [25]. SpaceX has claimed that each Starlink satellite contains three space lasers [26], i.e., 3-ISL configuration, which can maintain a global connection with less ISL ter-

minal cost. Although there is no public report indicating the exact ISL connectivity mode of Starlink, it is plausible and speculatively consistent that a 3-ISL topology is implemented, or partially implemented. A possible 3-ISL topology can be obtained by alternatively pruning inter-plane ISLs from the typical 4-ISL topology [25], then each satellite can maintain two intra-plane ISLs and one inter-plane ISL, forming a 3-ISL topology.

The 3-ISL topology has unique topological features. However, this new topology is less studied in satellite network areas. Although some researchers investigate similar topologies in mathematical theory [27] or chip field [28], they focus on simple and most regular cases, and the applicability is limited. Some properties in the 3-ISL topology should be similar to the 4-ISL case, while the differences are implicit and unknown. Note that pruning ISLs can not avoid the usage of inter-plane ISLs, but if the network can still perform comparably, then the reduced ISLs can save much cost. Thus, dedicated studies on the 3-ISL topology and routing issues in satellite networks are required.

Motivated by the above, this paper, for the first time, investigates the routing properties and performance of LEO mega-constellation networks with 3-ISL topology. Here, the routing property refers to the inherent features and fundamental behaviors of the path routing which will be theoretically derived and numerically verified. We focus on the derivation of fundamental routing metrics and properties, and the performance differences between the 3-ISL and traditional 4-ISL topologies, especially in mega-constellations. The main contributions are summarized as follows.

- By alternately pruning inter-plane ISL from traditional 4-ISL topology, the 3-ISL topology is obtained. A unified graph-based model and indexing scheme are formulated based on the revision of the 4-ISL model.
- Key network metrics and routing properties of the 3-ISL network topology are derived, including hop-count, network diameter, network cost, average path distance, etc. The model and properties are proven in Mesh and Torus topologies, respectively, and the differences are compared with the 4-ISL topology.
- By converting the 3-ISL topology into a honeycomb pattern, and introducing a ternary-indexing scheme, the shortest path searching region and path diversity are explicitly deduced.
- The propositions are numerically verified and leveraged to analyze the simulation results. Results indicate that the 3-ISL topology may cause more path distance, higher delay, and lower capacity, compared to the traditional 4-ISL topology. But the degraded performance depends on the constellation pattern, where constellations with fewer planes are preferred.

In the rest of the paper, Section II establishes the complete model, and Section III derives key routing properties for the 3-ISL topology. Section IV further investigates the shortest routing searching region and path diversity. Finally, Section V verifies the propositions and properties and further compares the performance between 3-ISL and 4-ISL topologies.

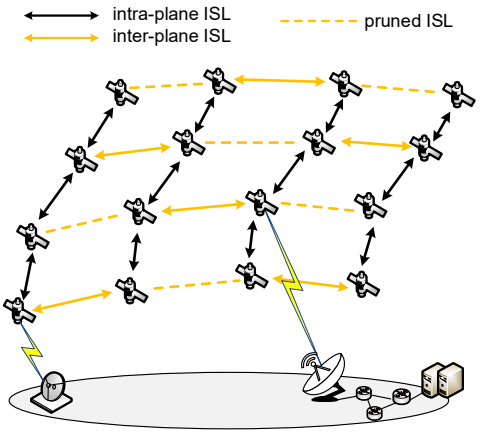

Fig. 1. Satellite network model with 3-ISL topology.

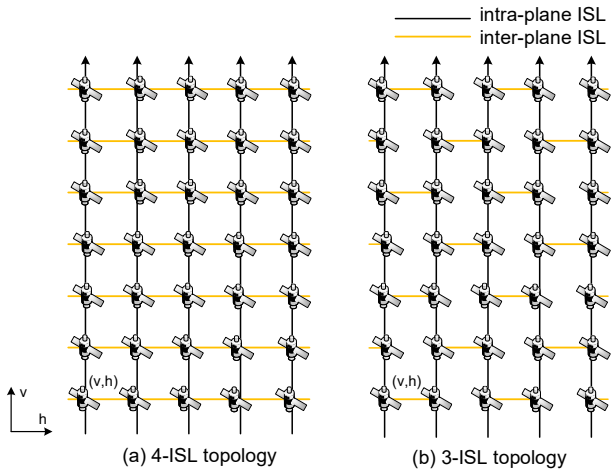

Fig. 2. Network topologies of the 4-ISL and 3-ISL patterns.

II. Network Model of the 3-ISL Topology

In this section, the LEO constellation network model and ISL topology are introduced, then the 3-ISL topology is generated and modeled by pruning half inter-plane ISLs, as shown in Fig. 1.

LEO constellations widely adopt the Walker-type which is regular and symmetric [9], [14], and can be denoted as $\alpha : N_P M_P / N_P / F$, where N_P orbit planes are distributed evenly along the equator, M_P satellites are evenly distributed in each plane, α is the orbit inclination, and phasing factor F specifies the relative spacing between satellites of adjacent orbits [12].

Satellite in a constellation can be indexed by (v, h) which indicates the v-th satellite in h-th orbital plane. Traditionally, in the 4-ISL pattern, each satellite establishes four ISLs with its neighbors: two intra-plane ISLs with the front and rear satellites within the plane and two inter-plane ISLs with the left and right neighboring satellites, respectively.

To reduce the usage of inter-plane ISLs and the cost of laser terminals, some inter-plane ISL terminals are pruned in some constellation proposals. In a pruned-ISL topology,

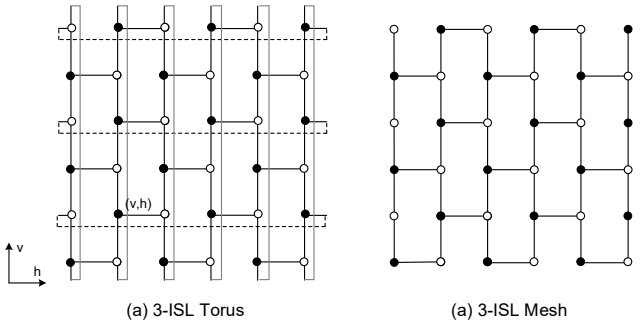

Fig. 3. Torus and Mesh of the 3-ISL topology.

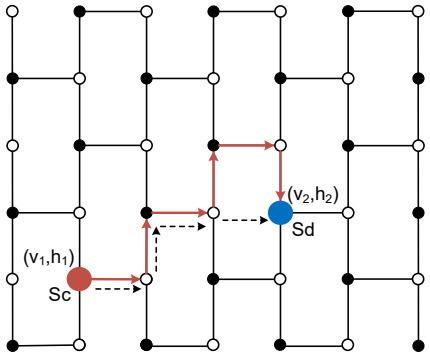

Fig. 4. Shortest path from Sc to Sd in the 3-ISL topology. Extra hops are required compared to the unpruned 4-ISL topology, which is indicated by the dashed path.

each satellite retains three ISLs: two intra-plane ISLs remain unchanged, and it establishes one inter-plane ISL alternatively with its right and left neighbors. This pruned 'T-shaped' topology is named 3-ISL in this paper, forming a brick wall pattern that looks like alternatively pruned half of the inter-plane ISLs from the classic 4-ISL topology, as shown in Fig. 2.

The 3-ISL network can be represented by graph $G = (\mathbf{V}, \mathbf{E})$, where $\mathbf{V}$ and $\mathbf{E}$ are the set of all satellites and links, respectively. $|\mathbf{V}| = N_P M_P$, and $|\mathbf{E}| = \frac{3}{2} N_P M_P$. Note that both N_P and M_P should be even to maintain a stable Torus topology. All the nodes have a degree of 3. According to the satellite moving direction and inter-plane ISL direction, the nodes can be divided into two groups. We define the even node set $\mathbf{V}_R = \{(v,h) \in \mathbf{V} \,|\, \mathrm{mod}\ (v+h,2) = 0\}$, where each node establishes an inter-plane ISL with its right neighbor, which is just an odd node. Similarly, the odd node set can be defined as $\mathbf{V}_L = \{(v,h) \in \mathbf{V} \,|\, \mathrm{mod}\ (v+h,2) = 1\}$.

Specifically, when the satellite $(1,h)$ and (M_P,h) in the same plane are connected and satellite $(v,1)$ and (v,N_P) in adjacent planes are connected, then a 3-ISL Torus topology is formed. Otherwise, the topology with non-looped end nodes is named 3-ISL Mesh, as shown in Fig. 3. Typically, in LEO constellation networks, the satellites within the plane form a ring, and satellites across adjacent planes also form a ring, thus the Torus topology is widely adopted. In some special cases, e.g., polar constellations where a seam exists, semi-Torus topology is formed. But when discovering paths between two satellites, the searching region can be simplified into a Mesh topology. Based on the ISL connection and satellite indexing, the 3-ISL Torus is node symmetric, thus its topology properties can be derived from an arbitrarily selected node.

III. Routing Properties and Metrics of 3-ISL Topology

Based on the network model and satellite indexing scheme, this section derives key routing properties of the 3-ISL topology, which is similar but unique compared to the 4-ISL topology. Most of the differences are due to the vertical detour caused by the intermittently missing inter-plane ISLs. Key routing metrics are derived, including minimum hop-count, network diameter, network cost, and average path distance, as summarized in Table I.

A. Minimum Hop-count between Two Nodes

Firstly, this paper takes the transmission hop count as the primary routing metric to be minimized, rather than physical distance, which is also a common practice [13], [14], [29]. Additionally, the paper uses the minimum hop count as the main metric for evaluating the 'path distance' between any two satellites.

Fig. 4 shows a shortest path from source satellite Sc to destination Sd in the 3-ISL topology, the path consists of several intra-plane and inter-plane hops. The required inter-plane hops depend on the orbital plane difference. However, the intra-plane hops are caused by both the satellite index difference and the inter-plane hops. When inter-plane hops are required but the corresponding inter-plane ISL is pruned, a detour is caused, and extra intra-plane hops are involved, compared to the unpruned 4-ISL topology. Moreover, we notice that the involved extra hops also depend on the parity of the end nodes.

Lemma 1. *In 3-ISL topology, N inter-plane hops involve at least N_{inv} intra-plane hops. N_{inv} between satellite (v_1,h_1), (v_2,h_2) can be given by*

$$N_{\mathrm{inv}} = N + \frac{h_2 - h_1}{|h_2 - h_1|} \left(\mathrm{mod}(h_1+v_1,2) - \mathrm{mod}(h_2+v_2,2)\right) \quad (1)$$

Proof. Since the inter-plane ISLs are alternatively pruned and each node has only one inter-plane ISL, an inter-plane hop must be followed by an intra-plane hop. When (v_1,h_1), (v_2,h_2) are both even or odd nodes, N inter-plane hops involve at least N intra-plane hops. Assume $h_2 > h_1$, when (v_1,h_1) is odd and (v_2,h_2) is even, an extra intra-plane hop is required. While (v_1,h_1) is even and (v_2,h_2) is odd, one intra-plane hop can be saved, and at least $N-1$ intra-plane hops are required. When $h_2 < h_1$, a similar conclusion can be obtained, and (1) is obtained. □

According to Lemma 1, the minimum involved intra-plane hops $N_{\mathrm{inv}} = N$ or $N \pm 1$, which depends on the type of end satellite. It also indicates that in the 3-ISL topology, the more orbital planes are involved, the more intra-plane hops

TABLE I
KEY METRICS SUMMARY OF 3-ISL AND 4-ISL TOPOLOGIES.

	Number of links	Degree	Network diameter	Network cost
4-ISL Mesh	$2N_PM_P - N_P - M_P$	Max. 4	$N_P + M_P - 2$	$4N_P + 4M_P - 8$
4-ISL Torus	$2N_PM_P$	4	$\frac{N_P+M_P}{2}$	$2N_P + 2M_P$
3-ISL Mesh	$\frac{3}{2}N_PM_P - N_P - \frac{M_P}{2}$	Max. 3	$N_P - 1 + \max\{M_P - 1, N_p\}$	$3N_P + \max\{3M_P - 3, 3N_p\} - 3$
3-ISL Torus	$\frac{3}{2}N_PM_P$	3	$\max\left\{\frac{N_P+M_P}{2}, N_P\right\}$	$\max\left\{\frac{3}{2}(N_P + M_P), 3N_P\right\}$

are required. Next, the minimum hop-count of 3-ISL topology is derived in Mesh and Torus, respectively.

1) 3-ISL Mesh Topology:

Proposition 1. (Hop-count in 3-ISL Mesh). *In a 3-ISL Mesh, the minimum hop-count between satellite* (v_1, h_1) *and* (v_2, h_2) *is*

$$H^{3\mathrm{M}}=\max\left\{|v_2-v_1|, |h_2-h_1|+\frac{h_2-h_1}{|h_2-h_1|}OE\right\}+|h_2-h_1| \quad (2)$$

where $OE = \mathrm{mod}(h_1 + v_1, 2) - \mathrm{mod}(h_2 + v_2, 2)$.

Proof. The minimum hop-count is the sum of the inter-plane hop-count H_h and intra-plane hop-count H_v. Similar to the 4-ISL Mesh, $H_h = |h_2 - h_1|$. When $|v_2 - v_1| \geq |h_2 - h_1|$, the minimum H_v is also similar, $H_v = |v_2 - v_1|$. However, when $|v_2 - v_1| < |h_2 - h_1|$, according to Lemma 1, the extra intra-plane hops H_{inv} caused by inter-plane hops can be greater than $|v_2 - v_1|$. Therefore, H_v should be $\max\{|v_2 - v_1|, H_{\text{inv}}\}$. Then combining (1) and the above formula with the total hop-count calculation, (2) can be obtained. □

2) 3-ISL Torus Topology:

Proposition 2. (Hop-count in 3-ISL Torus). *In a 3-ISL Torus, the minimum hops between satellite* (v_1, h_1) *and* (v_2, h_2) *is*

$$H^{3\mathrm{T}} = \max\left\{H_v^0, \min\left\{H_{inv}^0, N_P - H_{inv}^0\right\}\right\} + H_h \quad (3)$$

where $H_h = \min\{|h_2 - h_1|, N_P - |h_2 - h_1|\}$, $H_v^0 = \min\{|v_2 - v_1|, M_P - |v_2 - v_1|\}$, *and* $H_{inv}^0 = |h_2 - h_1| + \frac{h_2-h_1}{|h_2-h_1|}(\mathrm{mod}(h_1 + v_1, 2) - \mathrm{mod}(h_2 + v_2, 2))$.

Proof. The difference between Mesh and Torus is that the links in a Torus form a ring, and the reverse forwarding direction also becomes available. Similar to the 4-ISL Torus, the required minimum inter-plane hop-count becomes $H_h = \min\{|h_2 - h_1|, N_P - |h_2 - h_1|\}$. The minimum intra-plane hop-count in 4-ISL Torus is $H_v^0 = \min\{|v_2 - v_1|, M_P - |v_2 - v_1|\}$. In 3-ISL Torus, the inter-plane hops also involve at least H_{inv} intra-plane hops. Considering the reverse direction, the minimum intra-plane hops involved are $H_{\text{inv}} = \min\left\{H_{\text{inv}}^0, N_P - H_{\text{inv}}^0\right\}$, where $H_{\text{inv}}^0 = N_{\text{inv}}$ can be obtained from (1). The minimum intra-plane hop-count in 3-ISL Torus is $H_v = \max\left\{H_v^0, H_{\text{inv}}\right\}$. Finally, summing H_h and H_v can yield (3) and prove the proposition. □

According to the above derivation, we also obtain the intra-plane hop-count $H_v^{3\mathrm{T}} = \max\left\{H_v^0, \min\left\{H_{\text{inv}}^0, N_P - H_{\text{inv}}^0\right\}\right\}$ and inter-plane hop-count $H_h^{3\mathrm{T}} = H_h$. Since intra-plane and inter-plane ISLs have different link performances, researchers can set their weights on-demand to obtain a weighed hop-count metric $\hat{H}^{3\mathrm{T}} = \omega_v H_v^{3\mathrm{T}} + \omega_h H_h^{3\mathrm{T}}$, where ω_v and ω_h are the weights of intra-plane and inter-plane ISLs, respectively.

3) Extra Hops of 3-ISL Compared to 4-ISL Topology: Since half of the inter-plane ISLs are pruned, some node pairs in the 3-ISL topology need extra hops to connect each other, which are 'detours' in the 4-ISL topology. Based on (1), the extra hops can be further specified. Similar to the 4-ISL topology [22], the shortest path discovering subgraph in a 3-ISL Torus topology can also be simplified into a 3-ISL Mesh topology (See Section IV for details). Therefore, here we focus solely on the 3-ISL Mesh topology to discuss the extra hops.

Corollary 1. (Extra Hops). *Compared to 4-ISL Mesh, the shortest path in 3-ISL Mesh between* (v_1, h_1) *and* (v_2, h_2) *requires additional* ΔH *intra-plane hops,* ΔH *is an even number and we have*

$$\Delta H = \begin{cases} 0, & \textit{if} \quad |h_2 - h_1| \leq |v_2 - v_1| \\ |h_2 - h_1| - |v_2 - v_1| + \dfrac{h_2 - h_1}{|h_2 - h_1|}OE, & \textit{else} \end{cases} \quad (4)$$

where $OE = \mathrm{mod}(h_1 + v_1, 2) - \mathrm{mod}(h_2 + v_2, 2)$.

Proof. $\Delta H = H^{3\mathrm{M}} - H^{4\mathrm{M}} = {H_v}^{3\mathrm{M}} + {H_h}^{3\mathrm{M}} - {H_v}^{4\mathrm{M}} - {H_h}^{4\mathrm{M}}$. According to the hop-count calculation equations in 3-ISL and 4-ISL topology, ${H_h}^{4\mathrm{M}} = {H_h}^{3\mathrm{M}}$, thus, inter-plane detour is not involved. $\Delta H = {H_v}^{3\mathrm{M}} - {H_v}^{4\mathrm{M}}$, then based on (2) and ${H_v}^{4\mathrm{M}} = |v_2 - v_1|$, when $|h_2 - h_1| \leq |v_2 - v_1|$, $|h_2 - h_1| + \frac{h_2-h_1}{|h_2-h_1|}(\mathrm{mod}(h_1 + v_1, 2) - \mathrm{mod}(h_2 + v_2, 2)) \leq |v_2 - v_1|$, $H^{3\mathrm{M}} = H^{4\mathrm{M}}$ and $\Delta H = 0$. Similarly, when $|h_2 - h_1| > |v_2 - v_1|$, $\Delta H = |h_2 - h_1| - |v_2 - v_1| + \frac{h_2-h_1}{|h_2-h_1|}(\mathrm{mod}(h_1 + v_1, 2) - \mathrm{mod}(h_2 + v_2, 2))$.

Furthermore, since the parities of $|h_2 - h_1| - |v_2 - v_1|$ and $\mathrm{mod}(h_1 + v_1, 2) - \mathrm{mod}(h_2 + v_2, 2)$ are consistent, ΔH is an even number. □

According to the above proposition, in the 3-ISL topology, when $|h_2 - h_1| > |v_2 - v_1|$, the shortest path requires more inter-plane hops, and the extra hops are even and approximately equal to $|h_2 - h_1| - |v_2 - v_1|$. It also indicates that if $|h_2 - h_1| \leq |v_2 - v_1|$, then no extra hops are required, and the distance is the same as in the 4-ISL case.

B. Network Diameter and Network Cost

Network diameter and network cost are key metrics to evaluate the network efficiency [30]. The network diameter manifests the transmission times of messages between nodes and is defined as the maximum distance between any two nodes in a network, $D = \max_{S_i, S_j \in \mathbf{V}} H(S_i, S_j)$.

Proposition 3. (Network Diameter). *The diameter of a $N_P \times M_P$ 3-ISL Torus is*

$$D^{3\mathrm{T}} = \begin{cases} \dfrac{N_P + M_P}{2}, if\ N_P \le M_P \\ N_P, if\ N_P > M_P \end{cases} \tag{5}$$

Proof. Based on the definition of diameter, the max of H needs to be solved. According to (3), $H^{3\mathrm{T}} = H_h + \max\left\{H_v^0, H_{\text{inv}}\right\}$. Then $\max H_h = \frac{N_P}{2}$ is achieved when $|h_2 - h_1| = \frac{N_P}{2}$. Similarly, $\max H_v^0 = \frac{M_P}{2}$ is achieved when $|v_2 - v_1| = \frac{M_P}{2}$, and $\max H_{\text{inv}} = \frac{N_P}{2}$ is achieved when $H_{\text{inv}}^0 = \frac{N_P}{2}$. Then max of $H^{3\mathrm{T}}$ is $\frac{N_P}{2} + \max\left\{\frac{M_P}{2}, \frac{N_P}{2}\right\}$, the proposition is proven. □

According to (5) , the network diameter can also be expressed by

$$D^{3\mathrm{T}} = \max\left\{\frac{N_P + M_P}{2}, N_P\right\} \tag{6}$$

The network cost is defined as the product of diameter and degree [30]. Then the network cost of 3-ISL Torus is

$$\mathrm{Cost}^{3\mathrm{T}} = \begin{cases} \dfrac{3\left(N_P + M_P\right)}{2}, & \text{if } N_P \le M_P \\ 3N_P, & \text{else} \end{cases} \tag{7}$$

Typically, there is a trade-off between degree and diameter. Accordingly, the network cost is adopted as an evaluation metric to balance the above two parameters. But based on Proposition 3, when $N_P \le M_P$, the diameter of the 3-ISL network remains the same as the 4-ISL, thus the network cost is reduced by 25 percent, which indicates that the transmission timeliness can be maintained with fewer links and less network cost. The above propositions also indicate that more orbital planes may cause a longer path and greater cost, even though the total satellite number is fixed.

Similar to the above Torus topology, the diameter of the 3-ISL Mesh can be derived. $D^{3\mathrm{M}} = N_P - 1 + \max\left\{M_P - 1, N_P\right\}$. Combining the above derivations and fundamental conclusions from existing studies [22], [27], the network diameter and network cost of the four typical topologies are summarized in Table I. It can be found that with fewer ISLs, the network cost with 3-ISL is reduced by approximately 25% compared to the 4-ISL topology. However, if the constellation has too many orbital planes, the opposite situation may occur.

Note that the above conclusions are based on the regular ISL-connecting pattern where the phasing difference between adjacent orbit planes is near zero and satellites connected by inter-plane ISLs have the same v-index. When phasing difference cannot be ignored, satellite (v, N_P) and $(v+U, 1)$ can be connected by inter-plane ISL as a shortcut, and the network diameter can be decreased.

C. Average Inter-node Distance

The transmission efficiency over the network can be enhanced by reducing the average inter-node distance (AID) [14]. AID is defined as the average path distance for all possible node pairs through the network. The AID of a network with n nodes is calculated by

$$L = \frac{1}{n\left(n-1\right)} \sum_{S_i \ne S_j} H\left(S_i, S_j\right) \tag{8}$$

where $S_i, S_j \in \mathbf{V}$, $H\left(S_i, S_j\right)$ is the distance between S_i and S_j. In a $N_P \times M_P$ 3-ISL Torus, since the topology is node-symmetric, (8) can be simplified to

$$L = \frac{1}{N_P M_P} \sum_{j \ne 1} H\left(S_1, S_j\right) \tag{9}$$

Due to the node-symmetric property, S_1 can be any satellite node in the 3-ISL Torus. We can assume S_1=$(1,1)$, then by calculating the sum of $H\left(S_1, S_j\right)$, we can obtain the average inter-node distance.

Firstly, we can obtain the average inter-node distance of a $N_P \times M_P$ dimension 4-ISL Torus, $L^{4\mathrm{T}} = \frac{M_P + N_P}{4}$, the proof is omitted. Then we introduce the extra hops from 4-ISL to 3-ISL Torus, $\Delta H\left(S_j\right) = H^{3\mathrm{T}}\left(S_1, S_j\right) - H^{4\mathrm{T}}\left(S_1, S_j\right)$. It is known that $H^{4\mathrm{M}} = \min\left\{\left|h_2 - h_1\right|, N_P - \left|h_2 - h_1\right|\right\} + \min\left\{\left|v_2 - v_1\right|, M_P - \left|v_2 - v_1\right|\right\}$. Then according to (3) , $\Delta H\left(S_j\right)$ can be formulated as (4), and we have $\Delta H\left(S_j\right) \ge 0$.

Proposition 4. (Average Path Length). *The average inter-node distance of a $N_P \times M_P$ 3-ISL Torus is*

$$L^{3\mathrm{T}} = \begin{cases} \dfrac{\left(N_P + M_P\right)}{4} + \dfrac{{N_P}^2}{12M_P} - \dfrac{1}{3M_P}, if\ N_P \le M_P \\ \dfrac{\left(N_P + M_P\right)}{4} + \dfrac{{N_P}^2}{12M_P} - \dfrac{1}{3N_P} - \dfrac{\left(N_P - M_P\right)^3}{12N_P M_P}, else \end{cases} \tag{10}$$

Proof. Since the topology is node-symmetric, we assume S_1=$(1,1)$ is at the center of the Torus, then the Torus can be divided into four similar parts. First, we focus on the right-upper part, where the index (v,h) satisfies $1 \le v \le \frac{M_P}{2}$, $2 \le h \le \frac{N_P}{2}$. Then, according to (4), when $v \ge h-1$, $\Delta H\left(v,h\right) = 0$, as the black nodes shown in Fig. 5. When $v < h-1$, $\Delta H\left(v,h\right) = h - v - \mathrm{mod}\ \left(h+v, 2\right)$, as the gray nodes shown in Fig. 5. Then the sum of the extra required hops in this part is $\sum \Delta H\left(v,h\right)$= $\sum_{h=3}^{N_P/2} \sum_{v=1}^{h-2} h - v - \mathrm{mod}\left(h+v, 2\right)$. Similar expressions in other three parts can also be obtained. Then for the whole network, we have $\sum \Delta H\left(v,h\right) = \frac{{N_P}^3}{12} - \frac{N_P}{3}$ for $N_P \le M_P$, and $\sum \Delta H\left(v,h\right) = \frac{{N_P}^3}{12} - \frac{M_P}{3} - \frac{\left(N_P - M_P\right)^3}{12}$ for $N_P > M_P$. Based on the average inter-node distance of 4-ISL Torus, its total inter-node distances sum to $\frac{\left(N_P + M_P\right) M_P N_P}{4}$. Then the total inter-node distances of the 4-ISL Torus sum to $\frac{\left(N_P + M_P\right) M_P N_P}{4}$+$\sum \Delta H\left(v,h\right)$. Finally, according to (9), the proposition is proven. □

According to Proposition 4, comparing the 4-ISL, we find the average distance of the 3-ISL Torus is increased by

$$\Delta L = \begin{cases} \dfrac{{N_P}^2}{12M_P} - \dfrac{1}{3M_P}, if\ N_P \le M_P \\ \dfrac{{N_P}^2}{12M_P} - \dfrac{1}{3N_P} - \dfrac{\left(N_P - M_P\right)^3}{12N_P M_P}, else \end{cases} \tag{11}$$

When $N_P = M_P$, $\Delta L = \frac{N_P}{12} - \frac{1}{3N_P} \approx 0.08N_P$, which means that the average distance of the 3-ISL Torus is slightly

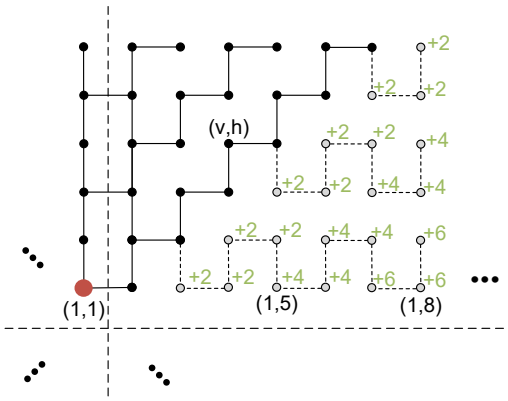

Fig. 5. Distribution of required extra hops from 4-ISL to 3-ISL Torus to reach (1,1), indicated by the green number besides hollow nodes.

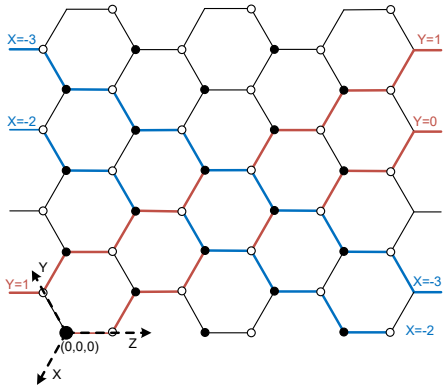

Fig. 6. Brick pattern can be converted to a honeycomb pattern.

increased compared to 4-ISL case. However, when there are too many orbital planes, the increased distance becomes more relevant. When $N_P > M_P$, $\Delta L = \frac{N_P}{4} - \frac{M_P}{4} + \frac{{M_P}^2}{12N_P} - \frac{1}{3N_P}$. When $N_P >> M_P$, $\Delta L \approx \frac{N_P}{4}$.

Furthermore, since the average hops of the inter-plane ISL are both $\frac{N_P}{4}$ for the two topologies, we can obtain the average hops of the intra-plane ISL, $L_{\text{intra}}^{\text{3T}} = L^{\text{3T}} - \frac{N_P}{4}$, i.e.,

$$L_{\text{intra}}^{\text{3T}} = \begin{cases} \frac{M_P}{4} + \frac{{N_P}^2}{12M_P} - \frac{1}{3M_P}, if\ N_P \le M_P \\ \frac{M_P}{4} + \frac{{N_P}^2}{12M_P} - \frac{1}{3N_P} - \frac{(N_P - M_P)^3}{12N_P M_P}, else \end{cases} \tag{12}$$

To sum up, the 3-ISL topology differs from typical 4-ISL topologies primarily due to the additional detours incurred when there are numerous inter-plane hops. Lemma 1 delineates the calculation of these extra hops. Subsequently, Propositions 1 and 2 provide explicit formulas for the hop-count in 3-ISL Mesh and Torus topologies, respectively. Based on this, Corollary 1 quantifies the increase in hop-count relative to the typical 4-ISL configurations. Finally, Propositions 3 and 4 determine the network diameter and AID for the 3-ISL Torus, respectively.

IV. Shortest Routing Discovery in the 3-ISL Topology

The last section focuses on the routing metrics for the overall network, then this section studies the routing discovery issue for the specific source and destination satellites. The 3-ISL topology is further converted into a honeycomb pattern, then path searching region and path diversity are formulated.

A. Shortest Path Searching Region

The shortest paths between two satellites are not unique, and the nodes on these multiple potential shortest paths form a shortest path searching region (SPSR). A node belongs to the SPSR if and only if it is an element of some shortest path between the two satellites. When the SPSR is determined, the shortest routing discovery becomes more efficient.

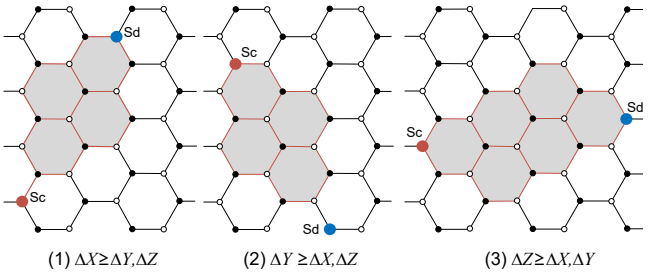

Fig. 7. Shortest path searching region between Sc and Sd.

Given the source satellite Sc and destination Sd, it can be known that for any intermediate satellite S_i within the SPSR, the sum of its distances towards Sc and Sd equals the distance between Sc and Sd. That is, if $S_i \in$ SPSR, then $H\,(Sc, Sd)$=$H\,(Sc, S_i) + H\,(S_i, Sd)$.

For a better illustration of the SPSR, we convert the network topology from the brick pattern into the 'honeycomb' pattern, as shown in Fig. 6. The intra-plane ISLs are staggered and tilted, forming a hexagonal honeycomb pattern. A triple-indexing scheme is introduced to facilitate the formulation of the SPSR. Similar to [27], [31], let the origin $(0, 0, 0)$ be at satellite node $(1, 1)$, and let X, Y, and Z axes be parallel to three edge directions, respectively. As shown in Fig. 6, the X-axis points in the direction where the satellite v-index decreases, the Y-axis points in the v-index increasing direction, and the Z-axis points in the h-index increasing direction. Then all nodes with a fixed (say) X, Y, or Z-coordinate belong to a zigzag chain. Then based on the indexing rules, the index (X, Y, Z) of neighboring satellite (v, h) can be given by

$$\begin{cases} X = \left\lceil 1 - \frac{v+h}{2} \right\rceil \\ Y = \left\lceil \frac{v-h}{2} \right\rceil \\ Z = h - 1 \end{cases} \tag{13}$$

Note that the index transformation only works in a Mesh topology. With the triple index, a honeycomb pattern is formed and its topological properties can be derived similar

to [27], [31]. The distance between Sc (X_1, Y_1, Z_1) and Sd (X_2, Y_2, Z_2) can be concisely given by $H = |X_2 - X_1| + |Y_2 - Y_1| + |Z_2 - Z_1|$. Then the hop-count in 3-ISL Mesh of (2) can also be calculated by

$$H^{3\mathrm{M}} = \left|\left\lceil -\frac{v_2+h_2}{2}\right\rceil - \left\lceil -\frac{v_1+h_1}{2}\right\rceil\right| + \left|\left\lceil \frac{v_2-h_2}{2}\right\rceil - \left\lceil \frac{v_1-h_1}{2}\right\rceil\right| + |h_2-h_1| \tag{14}$$

The above equations also indicate that the shortest path between these two nodes has $\Delta X = |X_2 - X_1|$ hops along X-axis, $\Delta Y = |Y_2 - Y_1|$ hops along Y-axis, and $\Delta Z = |Z_2 - Z_1|$ hops along Z-axis, respectively.

Then the SPSR can be specified by a group of several continuous hexagons, as shown in Fig. 7. The SPSR from Sc to Sd is limited by six zigzag chains, i.e., $X = X_1$, $X = X_2$, $Y = Y_1$, $Y = Y_2$, $Z = Z_1$, and $Z = Z_2$. Given the source satellite Sc and destination Sd, for any intermediate satellite S_i (X_i, Y_i, Z_i) within the SPSR, we have $X_1 \le X_i \le X_2$, $Y_1 \le Y_i \le Y_2$, and $Z_1 \le Z_i \le Z_2$ (assume $X_1 \le X_2, Y_1 \le Y_2, Z_1 \le Z_2$).

B. Shortest Path Diversity

The shortest path with minimum hops is not unique in the 3-ISL topology and is confined within the SPSR. The shortest path diversity can be calculated with ΔX, ΔY, and ΔZ.

Proposition 5. (Path Diversity). *The number of different shortest paths between two nodes in 3-ISL topology is*

$$K_{sp} = C\left(Hex_1 + Hex_2, Hex_1\right) \tag{15}$$

where $Hex_1 = \min\{\Delta X, \Delta Y\}$, $Hex_2 = \min\{\max\{\Delta X, \Delta Y\}, \Delta Z\}$, *and* $C(n,k)$ *is the number of combinations of* n *items taken* k *at a time.*

Proof. $Hex_1 = \min\{\Delta X, \Delta Y\}$ and $Hex_2 = \min\{\max\{\Delta X, \Delta Y\}, \Delta Z\}$ mean that Hex_1 and Hex_2 are the smaller two of ΔX,ΔY and ΔZ. Based on the 3-ISL topology and axis definition, the forwarding hops in the X, Y, and Z directions cannot be consecutive. For example, after a hop in the X direction, the next hop must be along either the Y or Z direction, and similarly for the other two directions. Assuming that the Z direction has the most hops, $\Delta Z > \Delta Y > \Delta X$, then it must be the case that $\Delta Z - (\Delta Y + \Delta X) = 0$ or 1.

On the other hand, the shortest path has totally $\Delta Z + \Delta Y + \Delta X$ hops, and before and after ΔZ hops in the Z direction, there must be one hop in the X or Y direction, which accounts for $\Delta X + \Delta Y$ hops. Therefore, each path can be determined by simply deciding the positions of ΔX hops in the X direction or ΔY hops in the Y direction. Then the total number of different paths is $K_{sp} = C\left(\Delta X + \Delta Y, \Delta X\right)$. When ΔX,ΔY and ΔZ satisfy other numerical relationships, this pattern also holds true, thus proving the proposition. □

Fig. 7 shows three cases of path diversity in the SPSR, we can find that $Hex_1 Hex_2$ are just the number of involved hexagons. Note that when Sc or Sd is near the marginal in a 3-ISL mesh, the path number will be reduced because the SPSR hexagons are truncated. But there is no marginal area in a 3-ISL torus, thus the above equations are more suitable for two nodes that are not too far apart in 3-ISL torus.

V. Simulations and Discussions

Through numerical simulations in various constellation scenarios, this section first verifies the proposed propositions and properties. Then the key network metrics of 3-ISL are evaluated and compared to the 4-ISL topology. Both user density distribution and multiple gateways are considered, and the effects caused by the pruned ISLs are further discussed.

A. Verification of the Propositions and Properties

To verify the proposed routing propositions and properties, the Monte-Carlo simulation method is adopted. Scenarios are established with different N_P and M_P ranging from 4 to 100. In each scenario, all the node pairs are traversed and examined. When $N_P M_P > 1000$, up to 1×10^6 node pairs are randomly selected for examination.

The Dijkstra algorithm is adopted to generate the shortest path between the node pairs as a benchmark for verification. Then the routing metrics of the 3-ISL topology, including hop-count, network diameter, and AID, are compared to the theoretical formulation. Results indicate that there is no error, confirming the accuracy of the proposed propositions and properties. Furthermore, when the path diversity is examined, slight deviations may occur in the 3-ISL Torus topology. Because the Torus topology enables paths in the opposite direction, extra paths may occur. But if the paths are limited within the Mesh topology, then this issue is avoided. Note that the related formulas of the 4-ISL topology have been well studied and examined and are not further discussed in this paper.

B. Network Performance Comparison between 3-ISL and 4-ISL Topologies

To investigate the network performance affected by the pruned ISLs, simulations are evaluated with the two ISL topologies in various constellations. Based on the basic Starlink phase-I constellation ($53°$@550km, $N_P = 72$, $M_P = 22$), six variant constellations are generated and tested. The 12×22, 24×22, and 36×22 configurations are with $\frac{1}{6}$, $\frac{1}{3}$, and $\frac{1}{2}$ of the total satellites of 72×22 case, 36×44 and 24×66 are the other two versions of the 1584-satellite configuration.

1) Hop-count Comparison: By selecting a central satellite and calculating its hop distances to all other satellites, the maximum and average inter-satellite hop distances are obtained, as shown in Fig. 8 and Fig. 9. Both two metrics exhibit similar trends. The maximum hop distance, or network diameter, grows linearly with the constellation scales, while in the 3-ISL topology, the maximum hop distance grows faster. Additionally, more orbital planes result in a higher maximum hop distance. In the 72×22 constellation, the 3-ISL topology may cause up to 35 additional hops compared to the 4-ISL case. This is due to the large inter-plane hops, which also necessitate many extra intra-plane hops. When the total satellite number is fixed and orbital planes are reduced, the

This article has been accepted for publication in IEEE Transactions on Aerospace and Electronic Systems. This is the author's version which has not been fully edited and content may change prior to final publication. Citation information: DOI 10.1109/TAES.2024.3512535

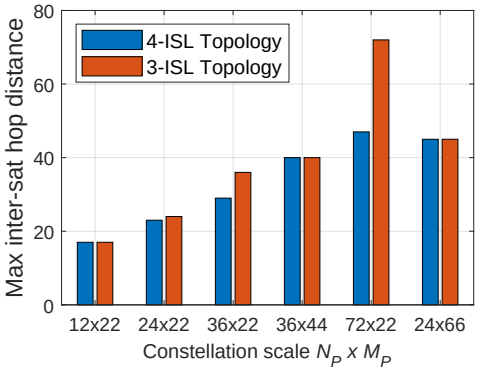

Fig. 8. Max inter-satellite hop distance of various topologies.

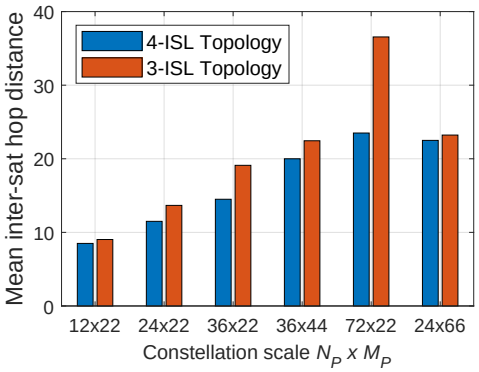

Fig. 9. Average inter-satellite hop distance of various topologies.

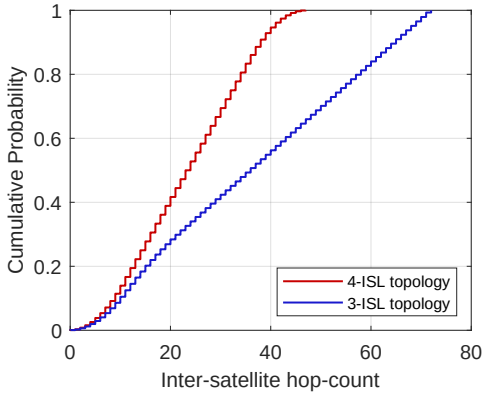

Fig. 10. CDF of hop-count in 72×22 constellation.

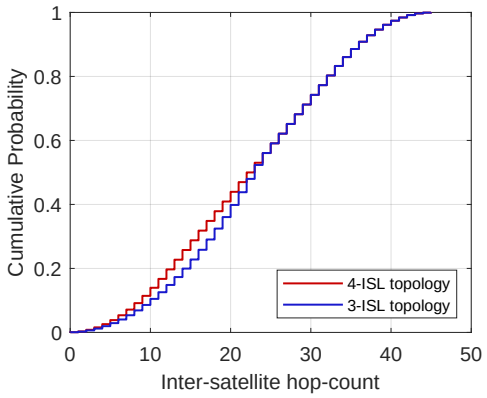

Fig. 11. CDF of hop-count in 24×66 constellation.

metric can be reduced to the same as in the 4-ISL case. These features match well with the formulated results in Table I.

As shown in Fig. 9, the average hop distance exhibits a similar trend to the maximum hop distance, while its value is approximately half that of the maximum value. This feature is consistent with those regular and uniform network topologies. Similarly, the average hop distance can be greatly reduced when more satellites are distributed in fewer orbit planes. Fig. 8, Fig. 9 and later Fig. 12 all indicate that the increase of N_P instead of M_P has more remarkable impacts on the network performance.

Fig. 10 and Fig. 11 present the cumulative distribution function (CDF) of the hop-count over the network for 72×22 and 24×66 constellations, respectively. It is evident that with an increased number of orbital planes, the required hop-count for the 3-ISL topology rises, and the hop-count distribution becomes more uniform. However, when the constellation configuration is adjusted to 24×66, the hop-count distributions converge significantly because detours can be avoided. In terms of the average hop distance, the metric increases by only 3.21%, even though 25% of ISLs are saved.

Since the ISLs become shorter, when the constellation is dense, the physical ISL distances as well as the link delays may not vary as noticeably as the hop-count. Fig. 12 illustrates the corresponding inter-satellite delay in different scenarios. We can observe that the delay remains relatively flat as the constellation scale increases. The total path length can be stable even if more intermediate satellites and hops are added. However, the delay also experiences a significant increase in the 3-ISL case when the constellation has more planes. In the 72×22 constellation, the delay has increased by more than double. But as long as $N_P < M_P$, the impacts of the pruned ISLs become much weaker (see the results of 36×44 and 24×66 cases).

2) End User Delay Comparison: We further consider the real satellite networks with a non-uniform distributed user density. These networks operate in an integrated space-terrestrial mode with multiple ground gateways. In this setup, satellites receive packets from end users and relay packets to their nearest gateway instead of all other satellite nodes as in the previous subsection, thus avoiding long ISL paths that can span half of the network. The satellite-gateway links utilize radio frequency (RF) links and do not occupy the ISL terminals. The user density distribution is determined by population demographics, and 30 gateways are strategically placed in proximity to user-dense regions to optimize the relay process [32]. The satellite receives data from ground users and forwards it to the nearest gateway station through inter satellite communication, in the entire network .

Table II lists the average end user delay when user density distribution and gateways are considered. Compared to Fig. 12 where all satellites become source-destination pair, the user delay is much reduced when gateways are introduced because only the nearest gateway becomes path destination

This article has been accepted for publication in IEEE Transactions on Aerospace and Electronic Systems. This is the author's version which has not been fully edited and content may change prior to final publication. Citation information: DOI 10.1109/TAES.2024.3512535

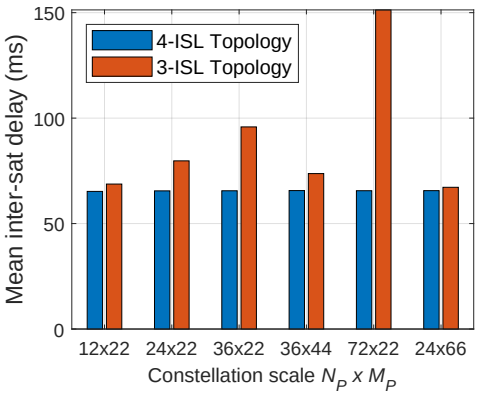

Fig. 12. Average inter-satellite propagation delay of various topologies.

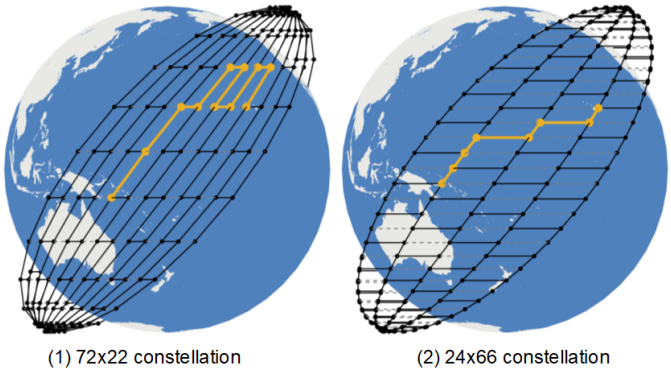

Fig. 13. Shortest path examples connecting Solomon Islands and Hawaiian Islands in different constellation configurations.

TABLE II
USER DENSITY-WEIGHTED DELAY WITH GATEWAYS.

		Average delay	User density-weighted average delay	Delay increase 3-ISL over 4-ISL
72×22	4-ISL	14.35 ms	10.42 ms	61.30%
	3-ISL	21.38 ms	16.80 ms	
24×66	4-ISL	14.52 ms	10.61 ms	3.00%
	3-ISL	15.09 ms	10.93 ms	
36×44	4-ISL	14.62 ms	10.64 ms	12.32%
	3-ISL	16.41 ms	11.95 ms	

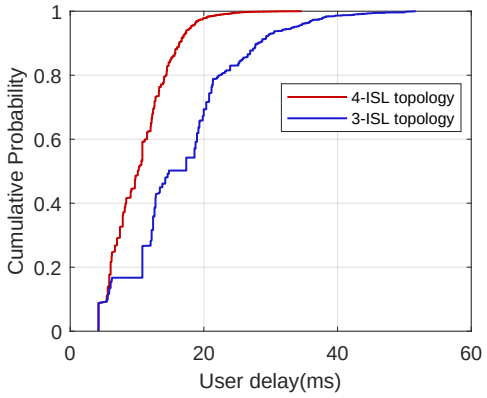

Fig. 14. CDF of user delay in 72×22 constellation.

and transmission path becomes shorter. Since the user density is non-uniform and the ground gateways are placed close to the user-dense regions, more packets can reach the gateway through shorter paths, resulting in lower average delay compared to a uniformly distributed user case. Thus, the user density-weighted average delay is further reduced. Comparing the 3-ISL and 4-ISL topologies, we find that the delay can increase by over 60% in the 72×22 constellation. But 24×66 is obviously a better design compared to other proposals, where the delay increases only 3.00% while 25% of the ISLs are saved.

Fig. 13 illustrates an example of a shortest path connecting the Solomon Islands and the Hawaiian Islands in different constellation configurations. Although the source and destination are the same, the path patterns are quite different. The hop-counts of the two paths are 10 for the 72×22 configuration and 7 for the 24×66 configuration, respectively. The two places are far away in the longitudinal direction and the 72×22 configuration has shorter inter-plane ISLs, thus more inter-plane hops are required and detours are caused. Moreover, intra-plane ISLs in the 72×22 configuration are longer, the increased delay is higher.

Fig. 14 and Fig. 15 further compare the CDF of delay in the two constellations. The 72×22 constellation suffers from extra detours when the inter-plane ISLs are pruned, the delay increases remarkably. But if the satellites are reorganized to the 24×66 configuration, the impact of the pruned ISLs on average delay becomes much smaller. Furthermore, the results of the 36×44 configuration in Table II indicate that when N_P becomes closer to M_P and the constellation is more regular, the impact of the pruned ISLs increases, but the degree of impact is still small. That is, $M_P > N_P$ is always preferred, and the greater M_P, the less impact is caused by the pruned ISLs.

3) Network Capacity Comparison: Since the network capacity is affected by the topology and average hops, the network capacity of various scenarios is also evaluated and compared. Mao et al. [29] have concluded that system capacity is inversely proportional to the average hop-count over the network, i.e., fewer hops cause higher system capacity.

The non-uniform user distribution and gateway placement are the same as in the above scenarios. The total user demand is set to 2 Tbps, the satellite-gateway link capacity is 20 Gbps, and the ISL capacity ranges from 1 to 10 Gbps. During the simulation, each satellite calculates the total user demand within its coverage area, which serves as the access traffic for this satellite. Then the capacity is evaluated using the max flow method [33]. At each time step, a maximum flow problem is constructed based on the constellation configuration, ISL connection topology, user traffic demand, inter-satellite links, and satellite-to-ground link capacities. We finally compute the maximum traffic that flows through all users to the ground gateways across the network, which is then adopted as the system capacity at that time step. The data in Fig. 16 represents the average system capacity over multiple time steps.

Fig. 16 shows that the capacity may decrease in the 3-ISL topology, but the effects are not as obvious as hop-count or

This article has been accepted for publication in IEEE Transactions on Aerospace and Electronic Systems. This is the author's version which has not been fully edited and content may change prior to final publication. Citation information: DOI 10.1109/TAES.2024.3512535

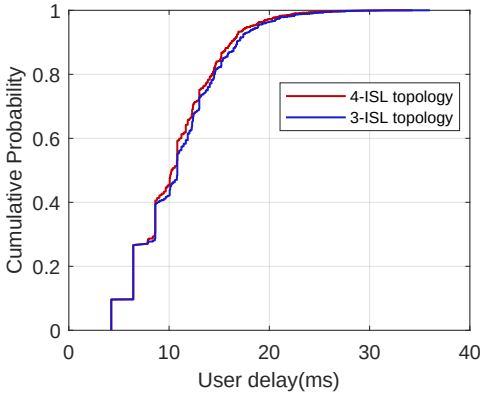

Fig. 15. CDF of user delay in 24×66 constellation.

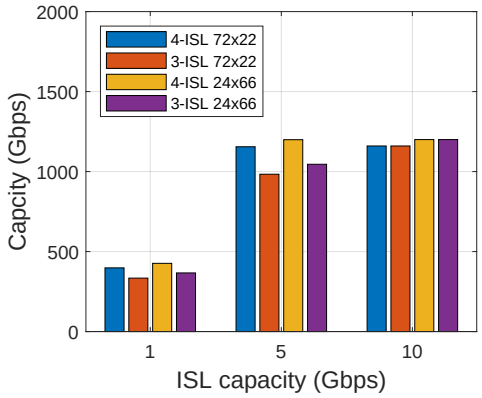

Fig. 16. Network capacity comparison of various topologies.

delay. The capacity degradation is around 15% when the ISLs are fully occupied. When the ISL capacity is large enough, the network capacity is limited by the satellite-gateway links. In these cases, the remaining ISLs are capable of routing the allowed traffic. Moreover, it is interesting that the various constellation configurations have very similar performance. The 24×66 configuration does not have more obvious advantages than the 72×22 configuration.

To summarize the simulation results, we find that the 3-ISL topology may degrade the network performance in terms of average hop-count, delay, network diameter, etc. But the degradation is affected by the constellation configuration. With fewer orbital planes and more satellites per plane, the pruned ISLs have weaker impacts on network performance compared to the typical well-connected 4-ISL topology. In a real satellite network with multi-gateway and user distribution, the performance degradation is also reduced. In terms of network capacity, when the ISL bandwidth is limited, the 3-ISL topology may further deteriorate network performance, but the degradation is not affected by the constellation configuration.

4) Irregularities in Actual 3-ISL Topology: In actual deployment of the 3-ISL topology in practice, irregularities may exist due to the satellite position deviation, node failures, ISL interruption, etc. First we consider the random satellite position deviation and node failures. We add a random deviation δu to the nominal phase of each satellite to simulate the actual satellite distribution, where $\delta u \sim \mathcal{N}(0, \sigma^2)$ and

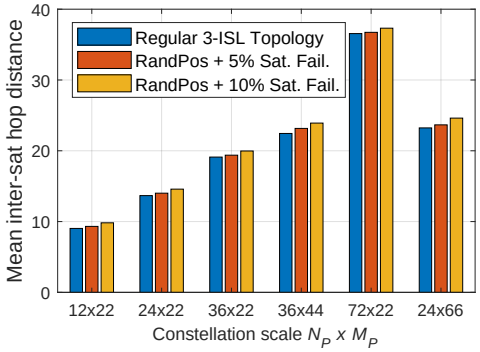

Fig. 17. Average inter-satellite hop distance of irregular 3-ISL topology with random satellite position deviations and satellite failures.

$\sigma = 1°$. Also, a specific proportion of satellites are randomly disabled as well as their ISLs. Fig 17 compares the effects of the irregular topology on the average hop-count. We can find that the average hop-count increases with the disabled satellite nodes. Compared to the regular 3-ISL topology, in all scenarios with 10% disabled satellites, the average hop-count increased by around 0.5 hops, but the relative deviation is relatively small, ranging from 2.08% to 8.77%.

The results in Table I are based on a regular topology. Results in Fig 17 indicate that in actual irregular LEO constellation scenarios, the results will be affected, depending on the number of missing node/links. But the impact is relatively small, and the conclusion is still applicable overall.

Considering the ISL maintenance issue, especially inter-plane ISL. It is influenced by the ATP (Acquisition, Tracking, and Pointing) system capability at the ISL terminal. As satellites in adjacent orbits pass before and after the orbital intersection point, the inter-plane ISL experiences a dramatic change in orientation. If the ATP supports tracking link pointing ranges, the ISL can be maintained at all times.

However, when the ATP fails to support the inter-plane ISL pointing range, the ISL needs to be interrupted and then reestablished after passing through the orbital intersection. At this point, we consider two scenarios: 1) Operational ISL model. The satellite carries 4 ISL terminals but only activates 3 to save resources. In this way, by dynamically and operationally rebuilding the link, the 3-ISL topology can be maintained. 2) Constructive ISL mode. The satellites are launched with only 3 ISL terminals. At this time, before and after each satellite pair passes through the orbital intersection, the inter-plane ISL connection status will switch, causing irregularity in the ISL topology near the orbital intersection points. However, outside of this area, a regular 3-ISL topology can still be maintained.

VI. Conclusions

This paper, for the first time, investigates the topological and routing properties of a pruned ISL topology in LEO constellation networks, i.e., the 3-ISL topology. Key routing properties are formulated and derived. The main feature is that the pruned inter-plane ISLs cause inevitable detours when the required inter-plane hops are more than intra-plane hops. The numerical

simulations verify the properties and indicate that the pruned ISLs may degrade network performance, especially hop-count. However, these impacts can be mitigated in real satellite network scenarios. A dedicated constellation configuration that distributes satellites more densely in each orbit, rather than across more planes, can lessen the impact. The theoretical frameworks and results can be used to analyze the impact of different ISL configurations on LEO constellations and guide the co-design of constellation pattern and ISL topology. More specifically, they can explain and analyze the advantages and disadvantages of the 3-ISL configuration compared to the typical 4-ISL configuration.

REFERENCES

[1] T. Ma, B. Qian, X. Qin, X. Liu, H. Zhou, and L. Zhao, "Satellite-Terrestrial Integrated 6G: An Ultra-Dense LEO Networking Management Architecture," *IEEE Wireless Communications*, vol. 31, no. 1, pp. 62–69, Feb. 2024.

[2] A. U. Chaudhry, G. Lamontagne, and H. Yanikomeroglu, "Laser Inter-satellite Link Range in Free-Space Optical Satellite Networks: Impact on Latency," *IEEE Aerospace and Electronic Systems Magazine*, vol. 38, no. 4, pp. 4–13, Apr. 2023.

[3] D. Zhou, M. Sheng, J. Li, and Z. Han, "Aerospace Integrated Networks Innovation for Empowering 6G: A Survey and Future Challenges," *IEEE Communications Surveys & Tutorials*, vol. 25, no. 2, pp. 975–1019, 2023-Feb.

[4] K. Han, B. Xu, S. Guo, W. Gong, S. Chatzinotas, I. Maity, Q. Zhang, and Q. Ren, "Non-Grid-Mesh Topology Design for MegaLEO Constellations: An Algorithm Based on NSGA-III," *IEEE Transactions on communications*, vol. 14, no. 8, 2024.

[5] S. R. Pratt, R. A. Raines, C. E. Fossa, and M. A. Temple, "An operational and performance overview of the IRIDIUM low earth orbit satellite system," *IEEE Communications Surveys*, vol. 2, no. 2, pp. 2–10, 1999.

[6] G. Jansson, "Telesat lightspeed™- enabling mesh network solutions for managed data service flexibility across the globe," in *2022 IEEE International Conference on Space Optical Systems and Applications (ICSOS)*, Mar. 2022, pp. 232–235.

[7] D. Bhattacherjee and A. Singla, "Network topology design at 27,000 km/hour," in *Proceedings of the 15th International Conference on Emerging Networking Experiments and Technologies*, 2019, pp. 341–354.

[8] A. U. Chaudhry and H. Yanikomeroglu, "Temporary Laser Inter-Satellite Links in Free-Space Optical Satellite Networks," *IEEE Open Journal of the Communications Society*, vol. 3, pp. 1413–1427, 2022.

[9] Q. Chen, G. Giambene, L. Yang, C. Fan, and X. Chen, "Analysis of Inter-Satellite Link Paths for LEO Mega-Constellation Networks," *IEEE Transactions on Vehicular Technology*, vol. 70, no. 3, pp. 2743–2755, Mar. 2021.

[10] M. Sheng, D. Zhou, W. Bai, J. Liu, H. Li, Y. Shi, and J. Li, "Coverage enhancement for 6G satellite-terrestrial integrated networks: Performance metrics, constellation configuration and resource allocation," *Science China Information Sciences*, vol. 66, no. 3, p. 130303, Feb. 2023.

[11] G. Barrenetxea, B. Berefull-Lozano, and M. Vetterli, "Lattice networks: Capacity limits, optimal routing, and queueing behavior," *IEEE/ACM Transactions on Networking*, vol. 14, no. 3, pp. 492–505, 2006.

[12] Q. Chen, L. Yang, Y. Zhao, Y. Wang, H. Zhou, and X. Chen, "Shortest Path in LEO Satellite Constellation Networks: An Explicit Analytic Approach," *IEEE Journal on Selected Areas in Communications*, vol. 42, no. 5, pp. 1175–1187, 2024.

[13] J. Sun and E. Modiano, "Routing Strategies for Maximizing Throughput in LEO Satellite Networks," *IEEE Journal on Selected Areas in Communications*, vol. 22, no. 2, pp. 273–286, 2004.

[14] Y. Lu, Y. Zhao, F. Sun, F. Yang, R. Liang, J. Shen, and Z. Zuo, "Enhancing transmission efficiency of mega-constellation LEO satellite networks," *IEEE Transactions on Vehicular Technology*, pp. 1–16, 2022.

[15] E. Ekici, I. F. Akyildiz, and M. D. Bender, "A distributed routing algorithm for datagram traffic in LEO satellite networks," *IEEE/ACM Transactions on Networking*, vol. 9, no. 2, pp. 137–147, 2001.

[16] G. Stock, J. A. Fraire, and H. Hermanns, "Distributed On-Demand Routing for LEO Mega-Constellations: A Starlink Case Study," in *2022 11th Advanced Satellite Multimedia Systems Conference and the 17th Signal Processing for Space Communications Workshop (ASMS/SPSC)*, Sep. 2022, pp. 1–8.

[17] X. Wang, W. Li, S. Han, M. Yang, and Z. Jiang, "Enabling High-Connectivity LEO Satellite Networks Via Encountering Inter-Satellite Links," in *GLOBECOM 2023 - 2023 IEEE Global Communications Conference*, Dec. 2023, pp. 4883–4889.

[18] W. Li, J. Liu, M. Sheng, and J. Li, "The capacity of k-connectivity d-dimensional wireless networks with node failure," *Science China Information Sciences*, vol. 66, no. 10, p. 209302, Sep. 2023.

[19] T. Shake, J. Sun, T. Royster, and A. Narula-Tam, "Failure Resilience in Proliferated Low Earth Orbit Satellite Network Topologies," in *MILCOM 2022 - 2022 IEEE Military Communications Conference (MILCOM)*, Nov. 2022, pp. 828–834.

[20] X. Xu, Z. Gao, and A. Liu, "Robustness of satellite constellation networks," *Computer Communications*, vol. 210, pp. 130–137, Oct. 2023.

[21] Z. Lai, H. Li, Y. Wang, Q. Wu, Y. Deng, J. Liu, Y. Li, and J. Wu, "Achieving Resilient and Performance-Guaranteed Routing in Space-Terrestrial Integrated Networks," in *IEEE INFOCOM 2023 - IEEE Conference on Computer Communications*. New York City, NY, USA: IEEE, May 2023, pp. 1–10.

[22] Q. Chen, L. Yang, D. Guo, B. Ren, J. Guo, and X. Chen, "LEO Satellite Networks: When Do All Shortest Distance Paths Belong to Minimum Hop Path Set?" *IEEE Transactions on Aerospace and Electronic Systems*, vol. 58, no. 4, pp. 3730–3734, Aug. 2022.

[23] W. Wang, Y. Zhao, Y. Zhang, X. He, Y. Liu, and J. Zhang, "Intersatellite Laser Link Planning for Reliable Topology Design in Optical Satellite Networks: A Networking Perspective," *IEEE Transactions on Network and Service Management*, vol. 19, no. 3, pp. 2612–2624, Sep. 2022.

[24] B. Soret and D. Smith, "Autonomous routing for LEO satellite constellations with minimum use of inter-plane links," in *2019 IEEE International Conference on Communications (ICC 2019)*, 2019, pp. 1–6.

[25] Y. Li, J. Wu, G. Kang, L. Chen, Y. Qiu, and W. Zhou, "A Flexible Topology Control Strategy for Mega-Constellations via Inter-Satellite Links Based on Dynamic Link Optimization," *Aerospace*, vol. 11, no. 7, p. 510, Jul. 2024.

[26] "Starlink: Satellite Technology," https://www.starlink.com/technology, 2024. Accessed: Oct-10-2024.

[27] I. Stojmenovic, "Honeycomb Networks: Topological Properties and Communication Algorithms," *IEEE Transactions on Parallel and Distributed Systems*, vol. 8, no. 10, 1997.

[28] U. A. Gulzari, Z. Salcic, W. Farooq, S. Anjum, S. Khan, M. Sajid, and F. S. Torres, "Comparative analysis of 2D mesh topologies with additional communication links for on-chip networks," *Computer Networks*, vol. 241, p. 110193, Mar. 2024.

[29] G. Mao, Z. Lin, X. Ge, and Y. Yang, "Towards a Simple Relationship to Estimate the Capacity of Static and Mobile Wireless Networks," *IEEE Transactions on Wireless Communications*, vol. 12, no. 8, pp. 3883–3895, 2013.

[30] J.-S. Kim, D. Kim, K. Qiu, and H.-O. Lee, "The divide-and-swap cube: A new hypercube variant with small network cost," *The Journal of Supercomputing*, vol. 75, no. 7, pp. 3621–3639, Jul. 2019.

[31] I. Stojmenovic, "Honeycomb networks," in *Mathematical Foundations of Computer Science 1995*, J. Wiedermann and P. Hájek, Eds. Berlin, Heidelberg: Springer Berlin Heidelberg, 1995, pp. 267–276.

[32] Q. Chen, L. Yang, J. Guo, X. Liu, and X. Chen, "Optimal Gateway Placement for Minimizing Inter-satellite Link Usage in LEO Mega-constellation Networks," *IEEE Internet of Things Journal*, vol. 9, no. 22, pp. 22 682–22 694, Nov. 2022.

[33] C. Jiang and X. Zhu, "Reinforcement Learning Based Capacity Management in Multi-layer Satellite Networks," *IEEE Transactions on Wireless Communications*, vol. 19, no. 7, pp. 4685–4699, 2020.

Quan Chen received the B.E. and Ph.D. degrees in aerospace engineering from the National University of Defense Technology (NUDT), Changsha, China, in 2015 and 2021, respectively. He is currently a lecturer with the College of Aerospace Science and Engineering, NUDT. His research interests include mega-constellation satellite networks, UAV networks, and integrated space-terrestrial networks. He has served as an associated editor for Telecommunication Systems.

Lei Yang received his Ph.D. degree in aerospace engineering from National University of Defense Technology, Changsha, China in 2008. Prof. Yang is currently a member of the Chinese Society of Astronautics and China Instrument and Control Society. His current research interests are focused on satellite communication networks, measurement and control technology for micro-satellite, on-board computer, spacecraft system modeling, and simulation.

Yong Zhao received Ph.D. degree in aerospace science and engineering from the National University of Defense Technology, Changsha, China, in 2005, where he is currently a professor. His research interests include micro/nano satellite design, spacecraft cluster application, and topological optimization.

Yi Wang received the Ph.D. degree in aerospace engineering from National University of Defense Technology, Changsha, China, in 2019. His current research interests include spacecraft dynamics and control, aerospace engineering and swarm intelligence.

Haibo Zhou received the Ph.D. degree in information and communication engineering from Shanghai Jiao Tong University in 2014. He is currently a Full Professor with the School of Electronic Science and Engineering, Nanjing University. He was a recipient of the 2019 IEEE Com Soc Asia-Pacific Outstanding Young Researcher Award, 2023–2024 IEEE ComSoc Distinguished Lecturer, and 2023–2025 IEEE VTS Distinguished Lecturer. His research interests include resource management and protocol design in B5G/6G networks, vehicular ad hoc networks, and space-air-ground integrated networks.

Xiaoqian Chen received his M.S. and Ph.D. degrees in aerospace engineering from the National University of Defense Technology, China, in 1997 and 2001, respectively. He is currently a professor of Chinese Academy of Military Sciences and an Academician of the Chinese Academy of Sciences (CAS). His current research interests include spacecraft systems engineering, advanced digital design methods of space systems, and multidisciplinary design optimization.